Supporting Information

A Comprehensive Computational Study of the Interaction between Human Serum Albumin and Fullerenes

Georgios Leonis,[a] Aggelos Avramopoulos,[a] Konstantinos D. Papavasileiou,[a] Heribert Reis,[a] Thomas Steinbrecher,[b] and Manthos G. Papadopoulos[a]

a. Institute of Biology, Pharmaceutical Chemistry and Biotechnology, National Hellenic Research Foundation, 48 Vas. Constantinou Ave., Athens 11635, Greece.
b. Institut für physikalische Chemie, Fritz-Haber Weg 2, KIT, 76131 Karlsruhe, Germany.

In the first section of the Supporting Information, the detailed methodology of clustering, secondary structure, dynamic domain, and FMO approaches is presented. In the second part, supplementary results include: a) structural investigation of the apo HSA as well as its complexes with compounds **2** (bound to the heme site) and C_{60}; b) AIM results for **2**; and c) energetic analyses (MM–PBSA, EDA, and FMO) for selected complexes to complement the findings shown in the main document. Compounds **1**,[1] **2**,[2] and **3**,[3] were taken from the respective references. The order of appearance of Figures and Tables herein coincides with the main text.

SI. Methods

SI.1 Clustering. This section details the complementary analysis performed for the 500 ns trajectories of **1**, **2**, and **3**–HSA complexes, as well as the HSA apo form. Specifically, cluster analysis was performed using the *gromos* algorithm[4] as implemented within the g_cluster utility of the GROMACS 4.6.4 software.[5] Trajectories were converted from the AMBER to the GROMACS format with the MDTraj program.[6] Atomic coordinates were extracted and the resulting 10,000 structures were superimposed with respect to their Cα atoms. Initially, the RMSD distance matrix of all Cα atom positions is calculated in a pairwise fashion. Cluster analysis proceeds by enumerating the structures having a calculated RMSD less than or equal to the predetermined cutoff (2.5 Å). Each structure is then clustered into a group, where the one having the smallest RMSD value serves as its center (cluster centroid). The entire cluster formed is in turn removed from the initial set; this process is repeated recursively until all structures are eliminated and assigned to a cluster.

SI.2 Secondary structure assignment. This was performed by means of the DSSP program.[7] HB analysis involved: a) all HSA, and b) i) IIA ii) IIIA and iii) heme binding site region residues. Regions i), ii) and iii) are described in detail below. The % secondary structure content of the systems was calculated as an average over 10,000 conformations.

SI.3 Dynamic domain analysis. To characterize the induced structural effect upon fullerenes' binding to HSA, the DynDom server was employed.[8] A detailed discussion on DynDom procedure is presented elsewhere;[8] for better understanding of the data presented herein, its main points are briefly summarized below:

- Initial identification of dynamic domains is achieved by comparing two structures of the same protein.
- These structures are superimposed by mass-weighted least-squares fitting of N, Cα, Cβ, and C atoms; either selected residues or the protein as a whole is considered.
- Atomic displacement vectors representing the rigid body movement of one domain (moving) relative to another (fixed) are determined.
- Clusters of residue rotation vectors are then calculated on each region by the K-means algorithm. Dynamic domains are assigned.
- Effective hinge axis describing the relative moving-to-fixed domain movement is then determined by Chasles' theorem; it passes near any of the inter-domain residues.[8]
- This axis can be decomposed into parallel and perpendicular components relative to the inter-domain center of mass joining line.
- The parallel axis describes a twist motion (twist axis); the perpendicular axis describes a closure motion (closure axis).[8] Following the definition by Hayward et al.,[8] a percentage measure of the degree of closure or twist motion can be defined from the square of the projection on either axis (e.g., % closure).

SI.4 The Fragment Molecular Orbital Method. For the FMO calculation of the HSA–fullerene complexes, HSA was split into fragments, where each fragment was composed of one residue, except if two residues were bound by S-S bonds, in which case the fragments consisted of these S-S bounded amino acids. For convergence reasons, the groups –NH-C(=O)– were not split at the N-C bond, but just outside the group, so that each fragment has a complete –NH-C(=O)– group. The fullerene was treated as a whole fragment. The HOP (hybrid orbital projection)[9] scheme was used as the bond detachment scheme for covalently bound fragments.

The fragments (monomers) were computed self-consistently at the 6-31G*/MP2 level, in the presence of the Coulomb field from all the other fragments. For the calculation of fragment interactions, all dimers were computed, at different levels of sophistication, according to the smallest distance between the monomers of the dimer: If this distance (corrected by van der Waals radii) was larger than 2 Å, only the electrostatic (including polarization) E_{es} interaction was computed. For R < 2 Å, a fully quantum-mechanical (QM) calculation was done, and the dimer interaction energy (ΔE_{int}) was further decomposed:

$$\Delta E_{int} = \Delta E_{es} + \Delta E_{ex} + \Delta E_{ct+mix} + \Delta E_{disp} \quad \text{(S1)}$$

Eq. S1 includes the usual terms of electrostatic (including polarization) energy ΔE_{es}, dispersion energy ΔE_{disp}, QM exchange energy ΔE_{ex}, and a rest term, which includes the charge-transfer energy plus several mixing terms (ΔE_{ct+mix}). The dispersion energy ΔE_{disp} is defined via the

difference between the (internal pair interaction) MP2 energy and the corresponding RHF energy. The amount of charge transferred between fragments (Q_{ct}) was also computed. **2** was docked in either IIA or IIIA, thus yielding two representative snapshots that correspond to the average geometries of the converged MD trajectories. These structures were used for the FMO analysis. To reduce the computational cost, the solvent surrounding each HSA–fullerene complex was reduced to a layer composed of all water molecules whose oxygen atom had a distance < 2.5 Å from the closest atom of the complex; this left 1541 water molecules. To investigate the water effect on the interactions, another calculation was done for **2**–HSA (in IIA only) without water. On this system, the effect of the radius between full computational and electrostatic treatment on the interactions was also investigated by increasing the value to 3 Å. It turned out that the additional terms computed in the full treatment were negligible for pairs with a radius between 2 and 3 Å.

In the Pair Interaction Energy Decomposition Analysis (PIEDA), a so-called PL0 state is defined as the state of a monomer in the electric field from all other monomers, and is composed of the sum of the destabilization energy due to mutual polarization and the stabilization due to electrostatic interactions between polarized charge distributions.[10] PL and 0 refer to polarization and free state, respectively. After computation of the PL0 state, the dimers are computed self-consistently, and the final state is denoted as the PL state. The interactions in the fully converged PL state differ from the PL0 state by several QM coupling terms, which are detailed in ref.[10]

SII. Results

Table S1. B–factors and radii of gyration for HSA complexes.

Compound	**B–factor (Å^2)** average/median	**Radius of gyration (Å)** average±STD deviation
1 in IIA	127.80/74.70	26.446±0.236
1 in IIIA	210.15/121.89	26.847±0.411
2 in IIA	133.96/87.39	26.606±0.170
2 in IIIA	157.48/75.80	27.253±0.204
2 in heme site	206.02/150.64	27.391±0.313
3 in IIA	170.06/77.14	26.443±0.244
3 in IIIA	103.70/66.81	26.303±0.144
C_{60} in IIA	153.94/78.04	27.321±0.178
C_{60} in IIIA	89.90/57.90	26.385±0.147
Apo HSA	163.78/94.61	27.433±0.398

SII.1 Conformational Analysis in apo HSA (500 ns MD run).

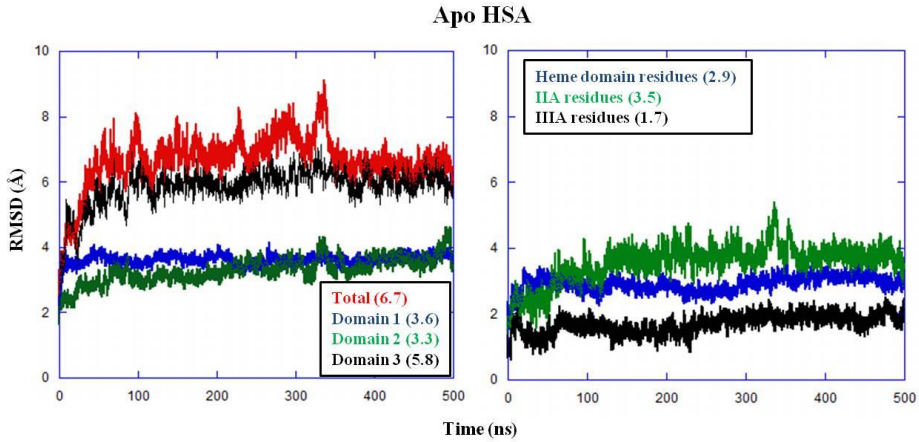

Figure S1. RMSD for Cα atoms of HSA residues in the apo form of the protein. RMSD plots are shown with respect to the entire protein, domain 1, domain 2, domain 3 and IIA, IIIA, and heme sites. Average RMSD values (in parentheses) are represented graphically in Figure 2 **(c)** and **(d)**.

SII.2 Conformational Analysis in HSA complexes with 1–3 and C_{60}.

SII.2.1 Conformational Analysis in Pristine C_{60}–HSA complexes (100 ns).

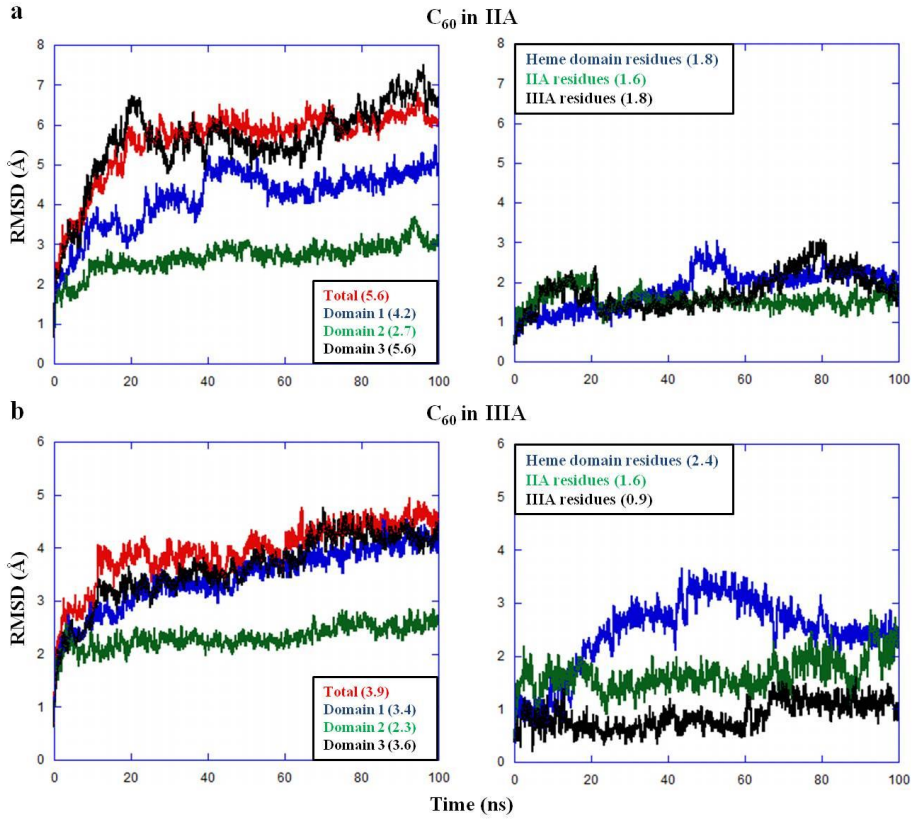

Figure S2. RMSD for Cα atoms of HSA residues with C_{60} fullerene core bound to **(a)** IIA and **(b)** IIIA sites. RMSD plots are shown with respect to: the entire protein, domain 1, domain 2, domain 3 and IIA, IIIA, and heme sites.

SII.2.2 Clustering analysis. Clustering was performed on the trajectories of complexes **1**–**3** and the apo form, using the RMSD of the Cα HSA atoms with a cutoff of 2.5 Å. Other cutoff values were also examined, but they produced clusters that were either too heavily or too poorly populated. The results are collected in Table S2. Cluster time evolution is depicted in Figure S3; Cluster ID:1 is the most prevalent during all simulations.

Table S2. Clustering results for **1**–**3** HSA systems using a 2.5 Å cutoff.

System	Number of clusters
Compound 1 in IIA	10
Compound 1 in IIIA	24
Compound 2 in IIA	10
Compound 2 in IIIA	28
Compound 3 in IIA	12
Compound 3 in IIIA	10
Apo HSA	23

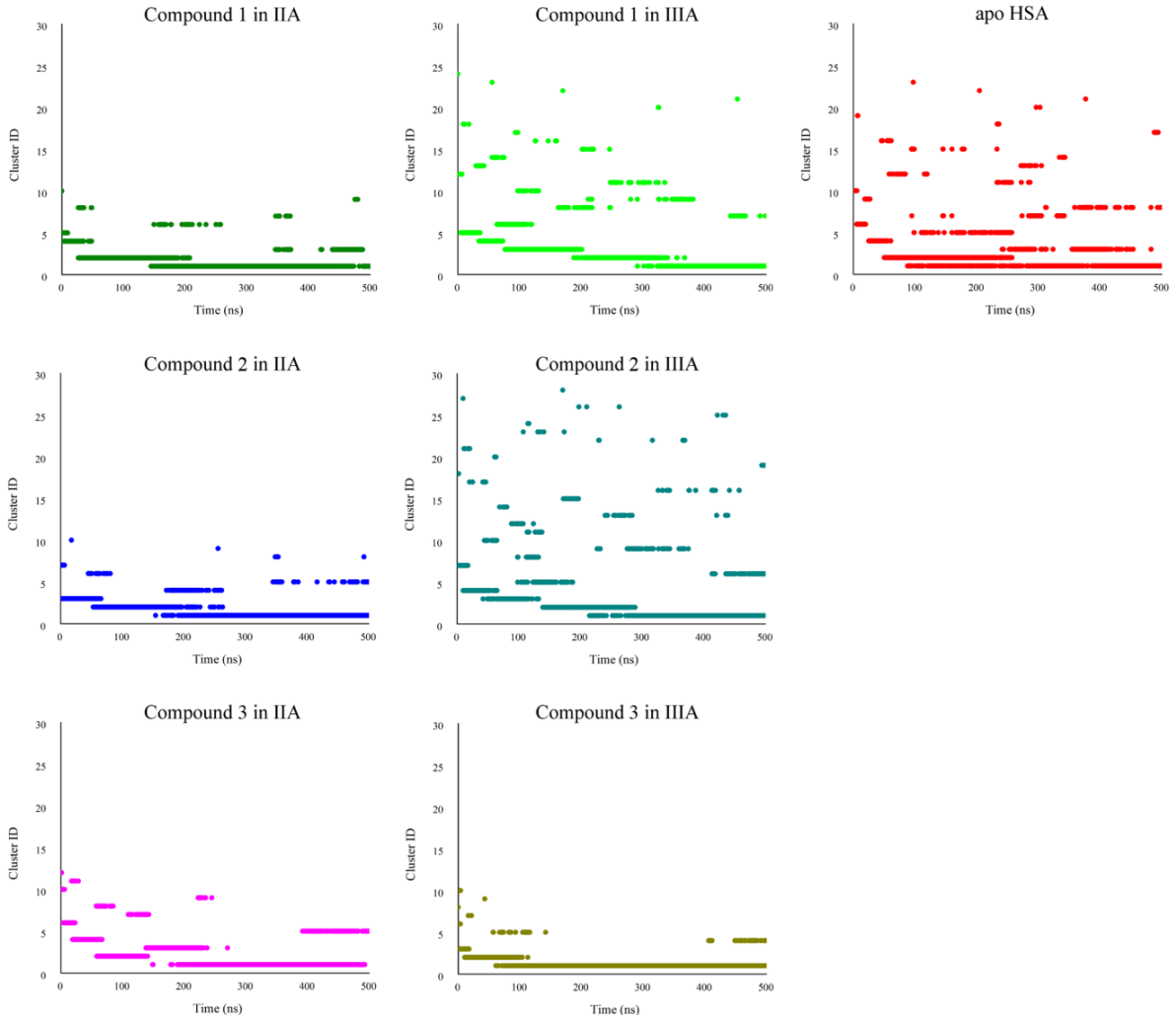

Figure S3. Population of clusters for compounds **1**–**3** vs. time in HSA IIA and IIIA sites as well as the HSA apo form. Cluster sequence numbers and their time distributions are shown.

SII.2.3 Secondary structure analysis (SSA). SSA was performed with the DSSP program[7] on 10,000 structures from the **1**–**3** trajectories and from the apo form. HSA regions were not limited to the binding site residues reported in the main text, but involved a broader selection:

i) IIA: Glu184–Ala194, Trp214–Pro224, His288–Asp297, His440–Ala449 (41 residues),
ii) IIIA: Glu383–Lys414, Leu430–Val433, Ala539–Leu544 (38 residues), and
iii) heme: Arg114–His146, Tyr161–Arg186 (59 residues).

The overall HSA secondary structure was mainly unaffected upon fullerene binding, however, inspection of binding regions revealed some changes. Besides the indication of allosteric modulation of the IIIA region upon binding to IIA (see main text), compounds **1**–**3** in IIA induce mixed effects: binding of **1** leads to a slight increase of IIA region's α-helical content by 2.2%, whereas binding of **2** and **3** leads to a 7.0% and 12.8% decrease, respectively (Figure S4c). Also, **2** binding to IIA increased the α-helical content at the heme region by 4.6%, whereas **1** and **3** lead to a decrease by 11.1% and 15.6%, respectively (Figure S4b). With regard to IIIA binding (Figure S4d), all compounds increased the helical and decreased the β-turn content compared to the apo form, without inducing any major changes to either IIA or heme binding sites. The only exception is **3**, which led to an increase of IIIA's β-turn content by 11.7% and a decrease of α-helical heme site's content by 11.5% (Figure S4b).

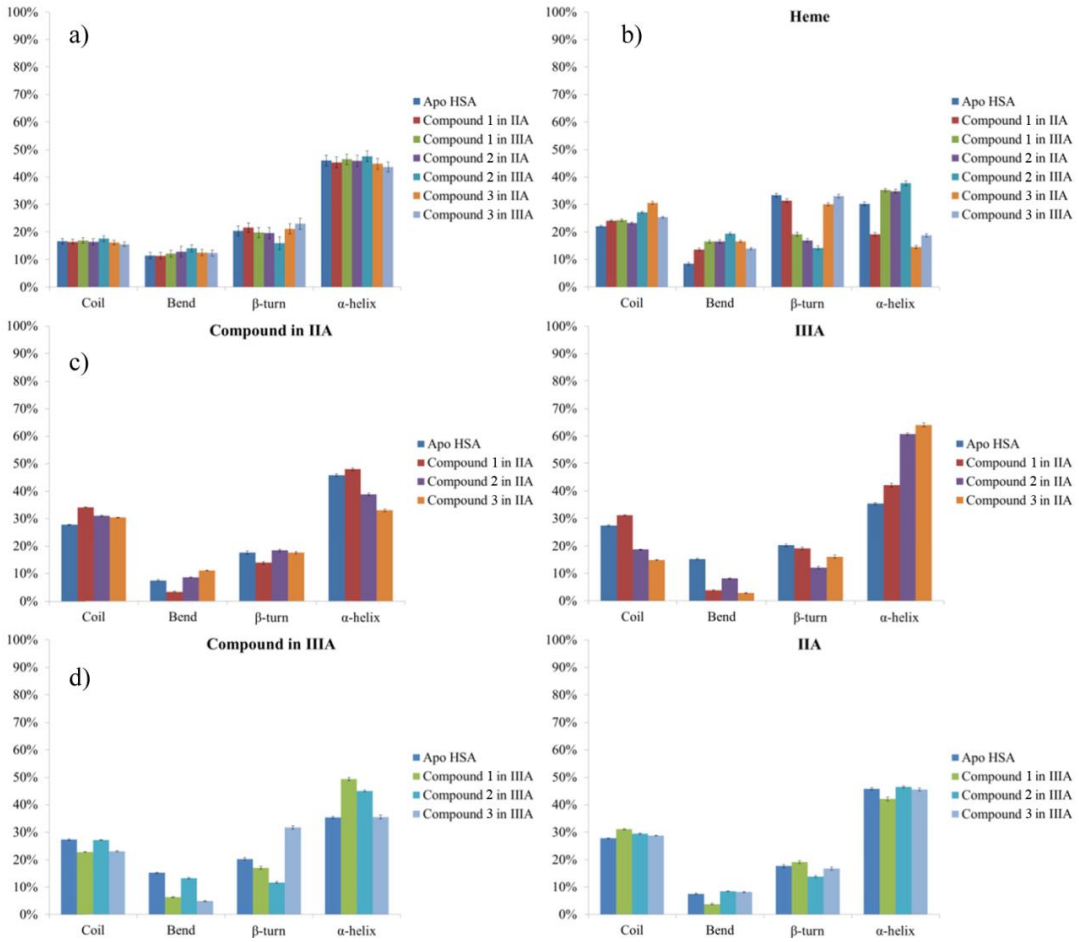

Figure S4. Percentage average secondary structure assignment for **(a)** entire HSA, **(b)** heme **(c)** IIA and **(d)** IIIA region residues, respectively, upon **1**–**3** binding. Only prevalent elements are shown; error bars are also depicted.

SII.2.4 Dynamic Domain Analysis (DDA). As described in the main text, clustering allowed the extraction of a small ensemble of representative HSA conformers, by partitioning the trajectories into distinct substates. Specifically, a comparison between the centroid structure of the longest living cluster (Cluster ID:1) and the crystal structure of HSA was performed to examine whether a large-scale molecular motion takes place. This involves movement of two (or more) protein domains as rigid bodies relative to each other. The structures of the longest living cluster can be thought as representative of all HSA systems, given their time span and their time signature, which lies toward the final part of all simulations. In other words, the hypothesis made is that HSA can be considered as adopting a conformation resembling that of the largest cluster's centroid. Results are presented in Figures S5-S8. The structure of Conformer 1 (1UOR) is in black, while the structure of Conformer 2 (Cluster ID:1) is in red. Hinge residues are colored green. The interdomain screw axis is in blue; the arrow head indicates the moving domain's direction of rotation according to the right-hand rule. Figure S6 illustrates the DynDom result for **1** at IIA site. Results for **3** at the IIA and IIIA sites are shown in Figures S7 and S8. The comparison of the apo HSA centroid conformer with the crystal structure, shown in Figure S5, requires particular mention. This conformational change is decomposed into three sets of rigid-body motions involving three protein segments (Domain A: 6–400, 406–497, Domain B: 401–405, 516–536 and Domain C: 504–515, 537–580, Figure S5a). The first movement involves rotation of Domain C with respect to B by 67.50° around a screw axis passing through residues 515–516 and 536–537. The second movement involves rotation of C with respect to A around residues 497–504 by 67.50°. The third rigid-body movement involves rotation and translation of B with respect to A by 70.00° and 5.20 Å, respectively. Finally, all distances between each screw axis and the center of mass (CM) of the domains were less than 5.50 Å; they are therefore effective hinge axes. The only exception is the apo form Fixed A (6-400, 406-497) and Moving C (504-515, 537-580) Domain screw axis (color code: blue tail–yellow head, CM-axis distance = 8.34 Å), which cannot be considered an effective hinge axis.

A movie describing the dynamic domain movements of HSA when **2** is bound to IIA (referring to Figure 6) was prepared by means of the Yale Morph Server[11] and VMD.[12]

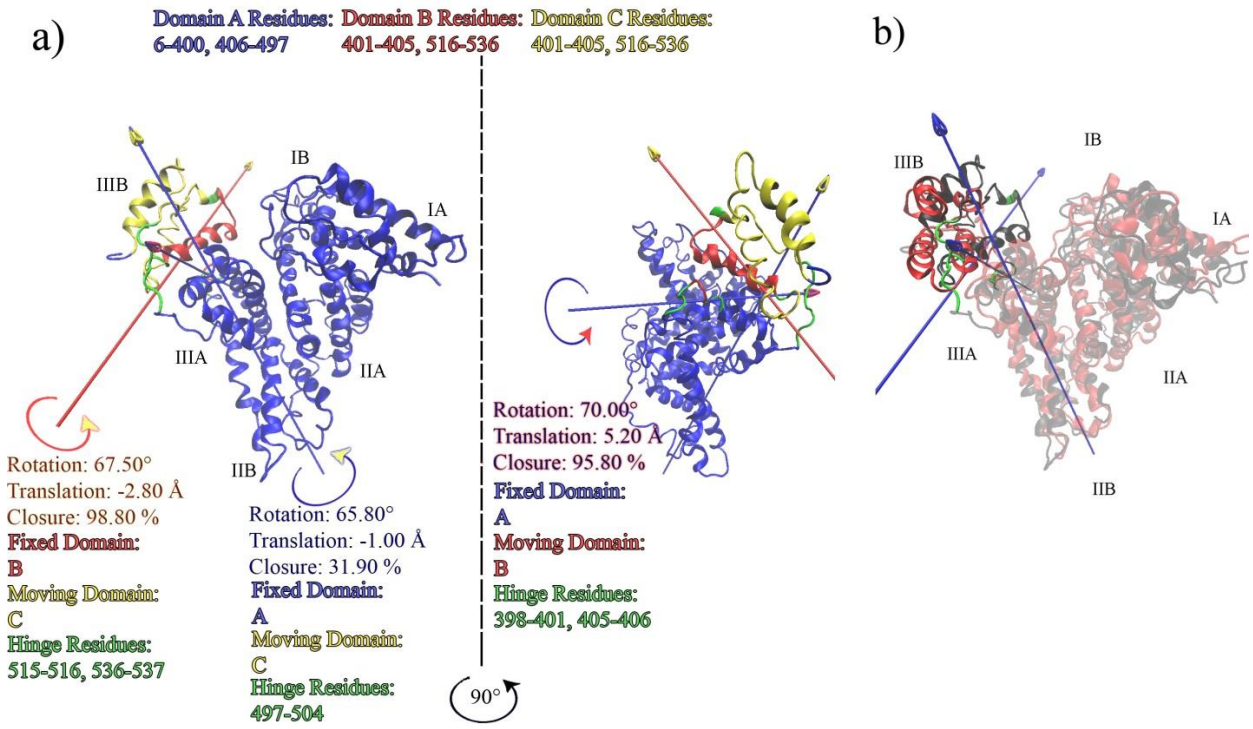

Figure S5. Results of dynamic domain analysis performed on the apo HSA. **(a)** Rigid body movement decomposition of IIIB subdomain. HSA structural segments (blue, red and yellow), hinge residues (green) and screw axes are illustrated; screw axes are color coded according to the protein segments involved, i.e., arrow tails and heads are colored according to fixed and moving domains, respectively. **(b)** Superposition of the apo HSA (Centroid ID:1, red) compared to the reference crystallographic structure (black).

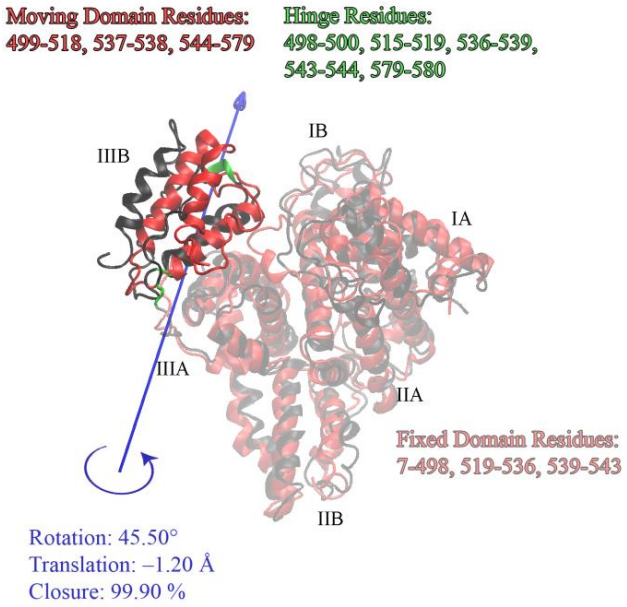

Figure S6. Results of dynamic domain analysis on HSA with **1** bound to the IIA site (red); the crystal structure is also depicted (black).

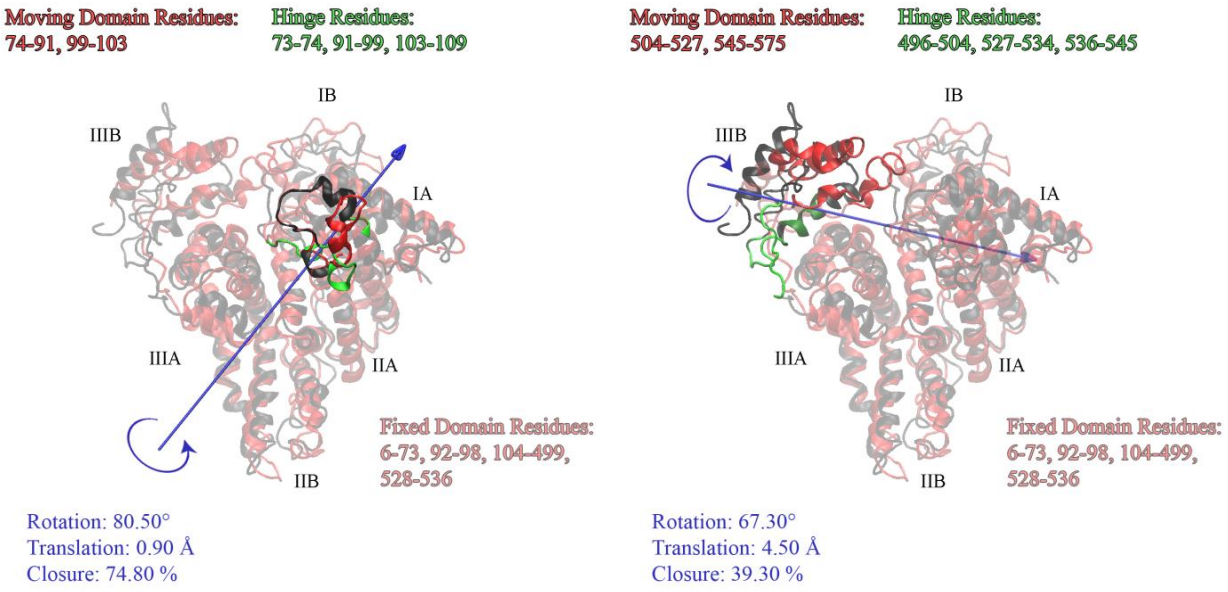

Figure S7. Results of dynamic domain analysis performed on HSA having compound **3** bound to the IIA site (red). Subdomain IA and IIIB motions are explicitly depicted.

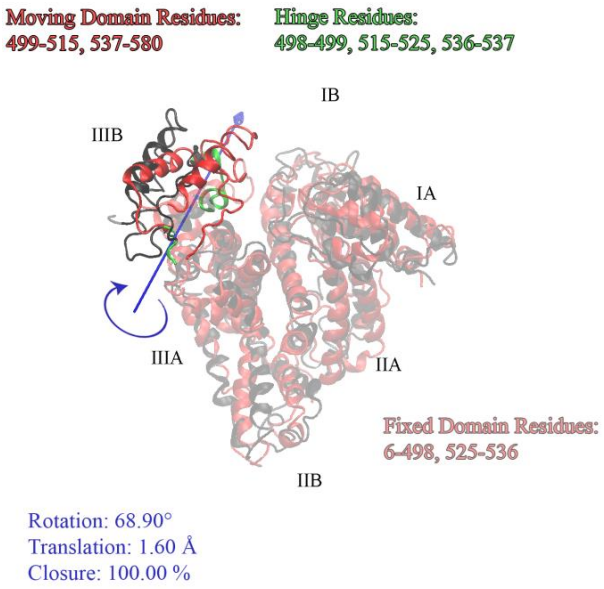

Figure S8. Results of dynamic domain analysis performed on **3**–HSA bound to IIIA.

SII.3 Atoms-in-Molecules Analysis. We used AIM to estimate the strength of the HBs in the **2**–HSA complex (IIA-bound form). The results (MP2/6-31G*) of the AIM analysis (Figure S9) yielded E(HB) values for HB1, HB2, –12.2 and –11.3 kcal/mol, respectively.

Figure S9. Hydrogen bonds (HB1, HB2) for the average structure of a truncated **2**–HSA system, as obtained by the early MD trajectory. The AIM method was used with MP2/6-31G* for the computation of the bond critical points. O, C, N and H atoms are shown in red, gray, blue and white, respectively.

SII.4 Conformational Analysis of 2 Bound to the Heme Binding Site of HSA (200 ns).

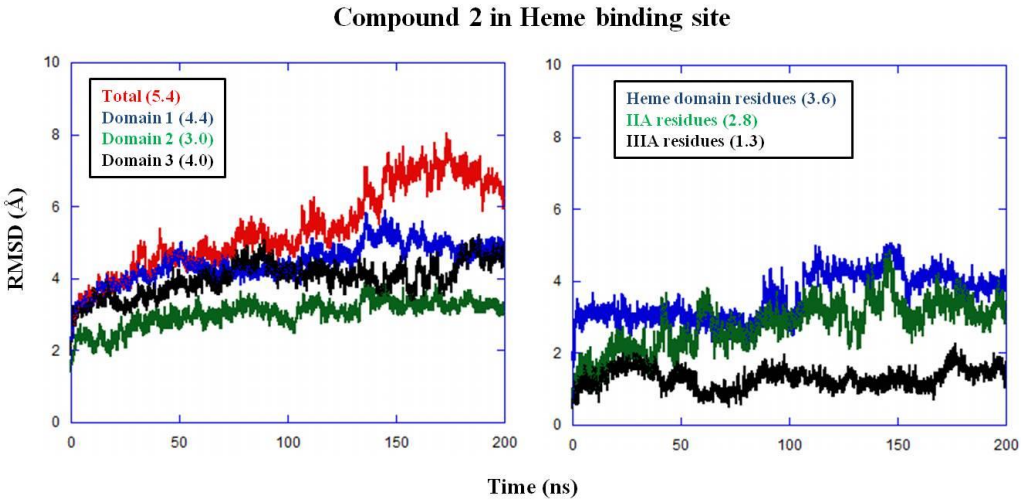

Figure S10. Cα RMSD of HSA residues with **2** bound to the heme site; averages in parentheses.

SII.5 Energy Decomposition Analysis.

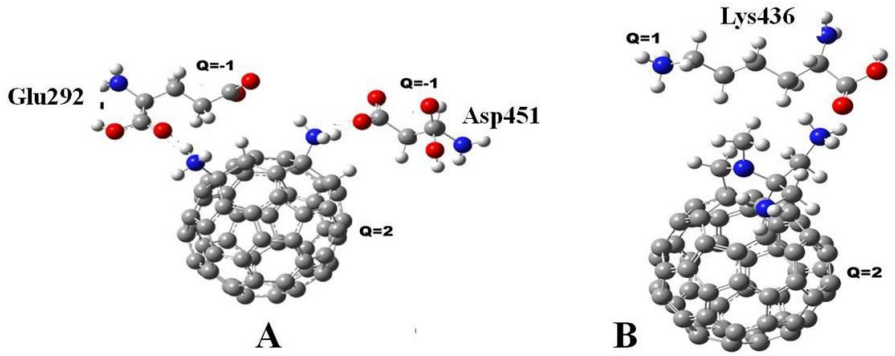

Figure S11. Fullerenes **2** (A) and **3** (B) interacting with IIA residues of HSA. The charge (Q) of each unit is reported. For atom color code, see Figure S9. The choice of residues (Glu, Asp, and Lys) was made according to the main HBs observed on the early-produced trajectories.

Table S3. Energetic analysis for HSA complexes with compounds **1**, **2** and **3**, as obtained by MM–PBSA calculations (Total simulation time: 500 ns for **1** and **3**, 550 ns for **2**).

	1[a]		**2**[a]		**3**[a]	
Energy (kcal mol^{-1})	IIA	IIIA	IIA	IIIA	IIA	IIIA
ΔE_{vdW}	–88.60±0.12[b]	–62.34±0.10	–48.95±0.03	–24.56±0.06	–60.99±0.03	–53.97±0.04
ΔE_{elec}	–82.23±0.54	–68.28±0.95	–272.66±0.39	–262.49±0.30	–375.59±0.38	–227.51±0.25
$\Delta E_{MM,\ gas}$	–170.83±0.52	–130.62±0.96	–321.60±0.39	–287.06±0.30	–436.59±0.38	–281.48±0.24
ΔG_{PB}	80.14±0.51	80.95±0.89	282.34±0.37	262.18±0.28	387.04±0.35	230.60±0.22
$\Delta G_{elec(tot)}$	–2.09±0.74	12.67±1.30	9.68±0.54	–0.31±0.41	11.45±0.52	3.09±0.33
ΔG_{NP}	–6.72±0.00	–5.39±0.01	–2.95±0.00	–1.09±0.00	–3.99±0.00	–3.50±0.00
ΔG_{solv}	73.43±0.51	75.55±0.89	282.34±0.37	262.18±0.28	383.06±0.35	227.10±0.22
$\Delta H_{(MM+solv)}$	–97.41±0.19	–55.07±0.17	–39.26±0.06	–24.88±0.03	–53.53±0.05	–54.38±0.05
$-T\Delta S_{tot}$	36.56±2.05	24.65±2.68	18.13±1.73	15.63±1.79	25.77±1.68	20.89±1.74
$\Delta G_{MM-PBSA}$	–60.85	–30.42	–21.13	–9.25	–27.76	–33.49

[a]Number of frames for enthalpy and entropy calculations is 12500 and 25, respectively (last 250 ns).
[b]Standard error of the mean.

Table S4. Decomposition of the interaction energy between **2** in IIA cavity and residues of HSA surrounded by a 2.5 Å water layer. When distance > 2.0 Å only electrostatics were computed. All energies are in kcal/mol.

Residue	Distance (Å)[a]	Electrostatics (E_{es})[b]		Charge Transferred (Q_{ct})[c]	Dispersion Energy (ΔE_{disp})	Exchange energy (ΔE_{ex})	Charge transfer energy + mixed terms (ΔE_{ct+mix})	Total interaction energy (ΔE_{int})[d]
		With water	Without water	With water / Without water	With water / Without water	With water / Without water	With water / Without water	With water / Without water
IIA								
Lys195	2.28	72.163 (2)[e]	67.737					
Gln196	2.54	–7.863	–7.568					
Lys199	2.91	69.342 (2)	65.835					
Trp214	2.72	2.109	0.117					
Arg218	1.16	98.256 (2)	97.020	–0.0006/ –0.0004	–0.975/ –0.942	0.034/ 0.030	–0.367/ –0.350	96.948/ 95.757
His242	3.11	–1.970	–2.947					
Arg257	3.47	52.678 (2)	51.107					
His288	2.76	0.054	–0.868					
Glu292	1.00	–110.372 (–2)	–107.762	–0.0049/ –0.0010	–5.237/ –5.332	3.077/ 3.113	–1.347/ –1.242	–113.879/ –111.223
Lys436	1.16	65.637 (2)	61.930	–0.0125/ –0.0132	–3.353/ –3.366	0.576/ 0.579	–1.036/ –1.087	62.871/ 58.057
His440	2.90	0.914	0.299					
Asp451	0.64	–155.610 (–2)	–153.789	0.0637/ 0.0866	–7.332/ –8.017	17.347/ 17.044	–6.433/ –7.906	–155.090/ –152.669
Ile523	8.69	0.268	0.130					
Gln543	14.07	–0.466	–0.384					
IIIA								
Glu321	9.91	–16.623 (–2)	–16.753					
Pro379	6.95	–1.153	–0.997					
Glu383	5.53	–33.925 (–2)	–33.553					
Gln390	4.78	–0.670	–0.360					
Asn391	3.73	–0.525	–0.618					
Leu407	5.21	0.525	0.591					
Arg410	6.49	27.679 (2)	27.354					
Tyr411	5.52	0.008	–0.065					
Lys413	8.28	21.348 (2)	21.063					
Lys414	6.87	29.072 (2)	28.231					
Leu430	3.45	–3.814	–3.425					
Val433	2.40	–3.102	–2.835					
Phe488	5.73	1.733	1.504					
Ser489	5.66	–0.136	–0.221					
Glu492	7.72	–23.812 (–2)	–23.624					
Heme Site								
Arg114	9.90	19.135 (2)	18.756					
Tyr138	6.61	–1.010	–0.883					
Glu141	6.49	–30.039 (–2)	–29.117					
Ile142	6.11	–2.322	–2.067					
His146	5.31	–2.622	–2.344					
Tyr161	5.60	0.733	0.612					
Ala171	10.09	0.571	0.467					
Leu185	4.47	–3.975	–3.175					
Arg186	4.71	27.815 (2)	27.550					
Tyr353	11.18	–0.114	–0.081					
Met548	15.63	–0.063	–0.061					

[a]Distance relative to van der Waals radii, namely distance = $R_{ij} - (R_i + R_j)$, where R_{ij} is the distance between i and j centers, and R_i, R_j are the van der Waals radii of i, j, respectively; [b]Including polarization; [c](Fullerene→i); [d]Total interaction energy = $\Delta E_{es}+\Delta E_{ex}+\Delta E_{ct+mix}+\Delta E_{disp}$
[e]The number in parenthesis is the product of charges (fullerene charge x residue charge).

Table S5. Decomposition of the interaction energy between **2** in IIIA cavity and residues of HSA surrounded by a 2.5 Å water layer. When distance > 2.0 Å only electrostatics were computed. All energies are in kcal/mol.

Residue	Distance[a] (Å)	Electrostatics (ΔE_{es})[b]	Charge Transferred (Q_{ct})[c]	Dispersion Energy (ΔE_{disp})	Exchange energy (ΔE_{ex})	Charge transfer energy + mixed terms (ΔE_{ct+mix})	Total interaction energy (ΔE_{int})[d]
IIA							
Lys195	7.24	26.638 (2)[e]					
Gln196	7.97	–1.294					
Lys199	7.53	22.498 (2)					
Trp214	5.82	0.114					
Arg218	6.90	25.116 (2)					
His242	8.75	0.923					
Arg257	10.68	18.218 (2)					
His288	12.52	–0.176					
Glu292	9.13	–23.552 (–2)					
Lys436	7.69	25.614 (2)					
His440	7.17	0.652					
Asp451	4.30	–30.435 (–2)					
Ile523	13.03	–0.319					
Gln543	10.50	0.497					
IIIA							
Glu321	9.82	–20.586 (–2)					
Pro379	0.98	–1.084	–0.0084	–6.162	4.577	–2.324	–4.994
Glu383	0.69	–145.900 (–2)	0.0503	–14.641	17.412	–7.554	–150.682
Gln390	1.86	3.099	0.0000	–0.422	–0.001	–0.017	2.659
Asn391	3.24	3.142					
Leu407	5.42	–0.710					
Arg410	4.74	30.603 (2)					
Tyr411	5.01	–0.833					
Lys413	5.95	24.704 (2)					
Lys414	3.67	41.340 (2)					
Leu430	4.98	–0.215					
Val433	5.49	0.762					
Phe488	2.87	1.142					
Ser489	2.02	3.328					
Glu492	1.90	–53.831 (–2)	0.0000	–0.297	–0.001	–0.003	–54.132
Heme Site							
Arg114	12.11	16.302 (2)					
Tyr138	14.17	–0.222					
Glu141	12.96	–16.528 (–2)					
Ile142	12.67	–0.232					
His146	10.89	–0.785					
Tyr161	15.36	0.171					
Ala171	18.38	0.031					
Leu185	11.19	–0.741					
Arg186	11.42	15.891 (2)					
Tyr353	8.22	–0.871					
Met548	15.79	–0.305					

[a]Distance relative to van der Waals radii, namely distance = $R_{ij} - (R_i + R_j)$, where R_{ij} is the distance between i and j centers, and R_i, R_j are the van der Waals radii of i, j, respectively; [b]Including polarization; [c](Fullerene→i); [d]Total interaction energy = $\Delta E_{es}+\Delta E_{ex}+\Delta E_{ct+mix}+\Delta E_{disp}$
[e]The number in parenthesis is the product of charges (fullerene charge x residue charge).

References

1. Friedman, S. H.; Ganapathi, P. S.; Rubin, Y.; Kenyon, G. L., Optimizing the binding of fullerene inhibitors of the HIV-1 protease through predicted increases in hydrophobic desolvation. *J Med Chem* **1998**, 41, 2424-2429.
2. Friedman, S. H.; Decamp, D. L.; Sijbesma, R. P.; Srdanov, G.; Wudl, F.; Kenyon, G. L., Inhibition of the Hiv-1 protease by fullerene derivatives - Model-building studies and experimental-verification. *J. Am. Chem. Soc.* **1993**, 115, 6506-6509.
3. Bosi, S.; Da Ros, T.; Spalluto, G.; Prato, M., Fullerene derivatives: an attractive tool for biological applications. *Eur. J. Med. Chem.* **2003**, 38, 913-923.
4. Daura, X.; Gademann, K.; Jaun, B.; Seebach, D.; van Gunsteren, W. F.; Mark, A. E., Peptide folding: When simulation meets experiment. *Angew. Chem., Int. Ed.* **1999**, 38, 236-240.
5. Hess, B.; Kutzner, C.; van der Spoel, D.; Lindahl, E., GROMACS 4: Algorithms for highly efficient, load-balanced, and scalable molecular simulation. *J. Chem. Theory Comput.* **2008**, 4, 435-447.
6. McGibbon, R. T.; Beauchamp, K. A.; Schwantes, C. R.; Wang, L.-P.; Hernández, C. X.; Harrigan, M. P.; Lane, T. J.; Swails, J. M.; Pande, V. S., *MDTraj: a modern, open library for the analysis of molecular dynamics trajectories*. **2014**.
7. Kabsch, W.; Sander, C., Dictionary of protein secondary structure: Pattern recognition of hydrogen-bonded and geometrical features. *Biopolymers* **1983**, 22, 2577-2637.
8. Hayward, S.; Berendsen, H. J., Systematic analysis of domain motions in proteins from conformational change: new results on citrate synthase and T4 lysozyme. *Proteins* **1998**, 30, 144-154.
9. D. G. Fedorov, K. K., *The fragment molecular orbital method: Practical applications to large molecular systems*. CRC Press: Boca Raton, **2009**.
10. Fedorov, D. G.; Kitaura, K., Pair interaction energy decomposition analysis. *J Comput Chem* **2007**, 28, 222-237.
11. Krebs, W. G.; Gerstein, M., The morph server: a standardized system for analyzing and visualizing macromolecular motions in a database framework. *Nucleic Acids Res* **2000**, 28, 1665-1675.
12. Humphrey, W.; Dalke, A.; Schulten, K., VMD: Visual molecular dynamics. *J Mol Graph Model* **1996**, 14, 33-38.